UNIVERSITY OF LATVIA

Summary of Doctoral Thesis

Reinis Baranovskis

INVESTIGATION OF ELECTROMAGNETICALLY DRIVEN FLOWS FOR DEGASSING PROCESS OPTIMIZATION IN LIQUID METAL

Riga, 2023

UNIVERSITY OF LATVIA

INVESTIGATION OF ELECTROMAGNETICALLY DRIVEN FLOWS FOR DEGASSING PROCESS OPTIMIZATION IN LIQUID METAL

Reinis Baranovskis
Advisor: Dr. phys. Ilmārs Grants

Submitted for the degree of Doctor of Physics
Subfield of Mechanics of Fluids and Gases

Riga 2023

The doctoral thesis was carried out at the University of Latvia, Faculty of Physics, Mathematics and Optometry, and in the Institute of Physics from 2019 to 2022.

The thesis contains an introduction, four chapters, a summary, and a reference list.

The form of the thesis is a dissertation in the field of physics and astronomy, in the sub-field of fluid mechanics.

Scientific supervisor: Dr. phys. senior researcher Ilmārs Grants

Reviewers:

1) Dr. phys. Guntars Kitenbergs (University of Latvia, Latvia)

2) Dr. sc. Aleksandrs Pedčenko (Coventry University, United Kingdom)

3) Dr. ing. Egbert Baake (Leibniz Universität Hannover, Germany)

The thesis will be defended at the public session of the Doctoral Committee of Physics and Astronomy at the University of Latvia, on March 24, 2023.

The thesis is available at the Library of the University of Latvia, Kalpaka blvd. 4.

Doctoral Committee of Physics and Astronomy in the University of Latvia

Chairman of the Committee: _____/ Dr. phys. Andris Jakovičs /

Secretary of the Committee: _____/ Sintija Siliņa /

ISBN 978-9934-18-933-3
ISBN 978-9934-18-934-0 (PDF)

Abstract

This thesis's motivation is improving one of aluminum's manufacturing steps - degassing. The excess dissolved gasses, such as hydrogen, are removed from molten aluminum during this stage. Currently, the most common way is to inject inert gas into the melt, and the gas absorbs dissolved hydrogen and leaves the metal through its free surface via bubbling. Existing methods need mechanical contact with the hot and chemically aggressive aluminum, leading to higher maintenance costs and heat losses. Here a novel contactless degassing method is researched. It uses electromagnetic forces to drive the flow, which disperses the injected inert gas bubbles. In this work, bubble dispersion by turbulent flow is studied experimentally in GaInSn and aluminum models. Bubble size reduction has been directly observed in liquid metal (GaInSn) and correlated with flow conditions. Velocity and pressure measurements are used to characterize fluid dynamics taking place in liquid metal. Power measurements describe electromagnetic performance and limitations of permanent magnet machines. These experimental results are further used to validate numerical MHD models developed parallel to this work. An experimentally validated numerical model calculates turbulence characteristics which can be used to express bubble size according to an empirical relation for bubble size in isotropic turbulence. Based on it, a method for predicting bubble refinement is proposed. This approach predicts bubble size in a proposed industrial aluminum prototype. Results show that refining bubbles in liquid metal with the electromagnetically created flow is possible. The impact in the aluminum industry covers 2500 aluminum smelting plants holding around 25 000 degassing units.

Keywords: Aluminum degassing, bubble collapse, dissolved hydrogen, metal stirring

Contents

1. Introduction

1.1. Motivation

Although aluminum is the world's second most used metal, some of its manufacturing steps have not been improved for decades. My thesis focuses on improving one of aluminum's manufacturing steps called "degassing". In a metallurgical environment, molten metal contains dissolved gases that cause mechanical defects like porosity that lead to worse mechanical properties [1]. To solve that, the concentration of dissolved gases must be reduced below a critical level before the molten metal is crystallized. The most common way is to inject inert gas in the melt, which absorbs dissolved hydrogen and leaves the metal through its free surface. Existing methods [2] need mechanical contact with the metal to disperse the gas into smaller bubbles and accelerate the degassing process. The contact with the hot and chemically aggressive aluminum leads to higher maintenance costs.

In my thesis, I propose to investigate a new contactless degassing method that uses an electromagnetic stirring system to create a suitable flow for the degassing process. The challenging task here is to ensure sufficiently turbulent flow while maintaining minimal free surface deformation. Solving these challenges requires extensive numerical and experimental modeling, which I aim to combine in this work. By improving such a vital step of aluminum manufacturing, the scope of impact would cover 2500 aluminum smelting plants holding around 25 000 degassing units, thus potentially seeing improvements in energy consumption, reduction in inert gas consumption, and an overall increase in efficiency.

1.2. Objectives of work

Aim of the work is to develop a novel degassing system using electromagnetically driven melt flow.

Objectives are:

- Perform literature analysis to understand the criteria for bubble collapse and the measuring methods for quantifying the degassing results.

- Develop a low-temperature experimental setup to test bubble dispersion by electromagnetically created flow using GaInSn alloy, which allows flow measurements for different degassing configurations. Use this setup to validate degassing potential of these configurations.
- Develop medium-scale aluminum experiments on bubble dispersion and demonstrate bubble refinement by the electromagnetically driven flow.
- Obtain experimental results for MHD numerical model validation. Develop a method that uses numerical model findings to predict bubble size in electromagnetically stirred aluminum.
- Predict industrial degassing unit operating parameters based on experimental findings.

1.3. Outline

To understand the degassing process, we shall first describe the fundamental physics behind it in section 2, which includes the formation, stability, and dynamics of gas bubbles in the liquid. Extra focus is put on specifying physical processes in the existing degassing methods and outlining the governing equations used for numerical calculations. In section 3, the literature analysis is presented, focusing on the existing degassing methods, the latest advances in them, and the newest research to put the proposed method in the context of the present situation in industry and science. The last subsection introduces permanent magnet machines and how they compare to other electromagnetic methods for metal transport. Section 4 introduces an experimental setup used to model degassing process in a laboratory scale and thoroughly explains measured parameters, their importance, and techniques used to obtain the results. Result analysis and discussion are presented in section 5, where the results of each measuring technique are shown together with the dimensionless analysis as part of the technology scaling process. The last section, section 6, summarizes obtained results, highlights the advantages and limitations of the proposed technology, and hypothesizes potential uses in the light alloy manufacturing industry.

1.4. Novelty

Rotating permanent magnet machines is a niche way to create rapid flow in molten metals. In this work, our experience in liquid metal stirring is applied to the problem of aluminum degassing. Most of the research on degassing is either done on aluminum (where resulting gas content is measured) or with water models. There are very few observations of bubble movement in liquid metal since visual observations are limited to x-rays and neutron imaging. The same is true about observing bubble movement in the presence of a magnetic field and current density because most liquids have negligible or no electrical conductivity. No other research groups have not attempted the proposed method of aluminum degassing. To author's best knowledge, bubble refinement by turbulent flow in liquid metal is observed for the first time. In this work, a new approach for predicting bubble size is utilized. An experimentally validated numerical model calculates turbulence characteristics which can be used to express bubble size according to an empirical relation for bubble size in isotropic turbulence.

2. Theoretical background

Bubble breakup in liquid metal by electromagnetic forces is a multiphysics problem containing multiple continuum mechanics branches. In this section, the established theory of the main aspects is discussed. Firstly, it is summarized how the gas solubility in metal establishes a need for degassing by introducing the sources of contamination and explaining hydrogen presence in aluminum. Secondly, since most degassing methods rely on inert gas injection, gas bubble stability in liquid metal is analyzed to understand the necessary criteria for bubble breakup. Thirdly, scientific literature uses many dimensionless numbers to characterize the system and compare various models. The most often used are discussed, and this study's value range is highlighted in Grace diagram. Lastly, governing electromagnetism and fluid mechanics equations are discussed. They form the foundation of equations that numerical methods use to solve the studied problem. Additionally, the main dimensionless groups characterizing electromagnetic stirring are defined here.

2.1. Gas solubility in metal

In industrial processes, aluminum inevitably dissolves hydrogen from water vapor in the environment. Adverse effects of dissolved hydrogen in various alloys are fundamentally explained in these papers [1, 3]. Aluminum collects hydrogen from water vapor and air in storage and processing. Naturally, the process is drastically faster when aluminum is molten, and its surface is agitated. Thus the most critical phase where the melt can be contaminated by hydrogen is the melting of aluminum by gas, where one of the combustion products is water.

Hydrogen content is measured in rather odd units of $\frac{\mathrm{cm}^3}{100\ \mathrm{g}}$. Above all, the dissolved hydrogen causes porosity even in trace amounts, leading to worse mechanical properties as shown in Fig. 2.1. The threshold where dissolved hydrogen causes significant porosity depends on the alloy and which manufacturing technique is being used. It is in range of 0.1 to 0.4 $\frac{\mathrm{cm}^3}{100\ \mathrm{g}}$ as can be seen in Fig. 2.1a. Converted to mass fraction values, the thresholds are tiny and in the range of $8.5 \cdot 10^{-5}$ to $3.5 \cdot 10^{-4}$; however, the porosity depends on volume fraction, which is in order of 10^{-2}. Graph in Fig. 2.1b clearly illustrates that porosity in order of 1 % dramatically decreases tensile strength.

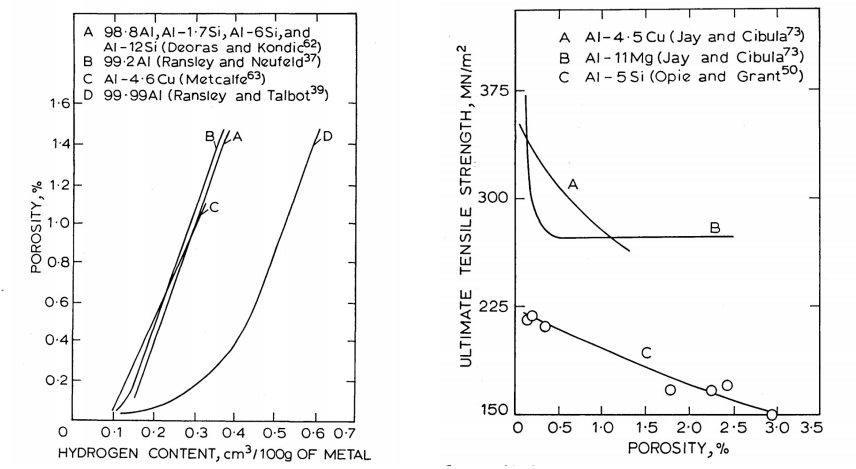

(a) **Porosity vs. hydrogen** *(b)* **Tensile strength vs. porosity**

Figure 2.1: **Effects of dissolved hydrogen on porosity and mechanical properties in sand cast aluminum and aluminum alloy bars** [1]

Therefore reducing hydrogen content (or simply degassing) is a necessary step before manufacturing the final aluminum product.

2.2. Bubble breakup in liquid

In Fig. 2.2, a Grace diagram is shown with the highlighted areas corresponding to experiments done within this thesis. According to it, we will see wobbling shapes which is reasonable since that is observed before the bubble collapse.

Froude number is expected to be considerably larger than unity - $Fr \gg 1$. This means that the inertial and centrifugal forces dominate, and the flow is supercritical (a flow whose velocity is faster than the wave velocity). Reynolds number is larger than 10^3 across the length scale, so we expect to be dealing with a turbulent flow. Eötvös number reaches parity at around 4 mm.

In such conditions, the only mechanism for bubble collapse is to create a pressure difference on the liquid-gas interface. In the case of a turbulent flow, the pressure changes come from the dynamic pressure of the liquid flow, which varies in time chaotically. The fundamental mechanism of bubble breakup is complicated. According to a highly cited article by

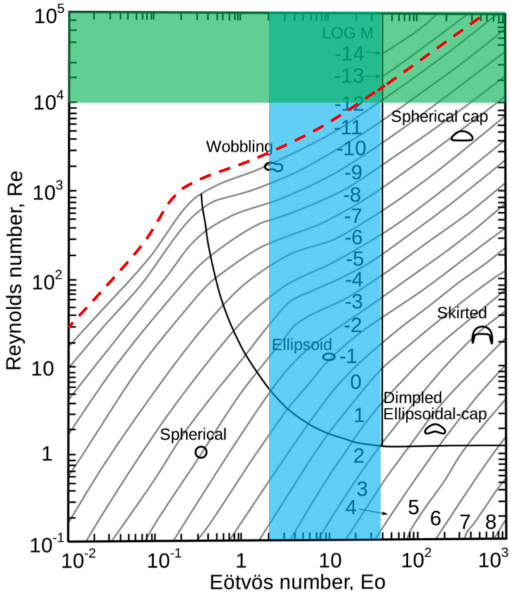

Figure 2.2: **Shape approximation to Reynolds, Eötvös, and Morton number [4]. Green shading represents a range of Reynolds numbers during our experiments, blue shading represents Eötvös number for bubbles from 4 to 20 mm, and the red dashed line is the logarithm of Morton number, taking into account GaInSn properties.**

Hinze [5] there are two sources of forces in flow, three types of deformation, and six main types of flows around a globule. Two dimensionless numbers characterize the condition of the flow. The first one is Weber number (2.1) which describes the ratio of drag force to surface tension force.

$$We = \frac{\rho v^2 l}{\gamma} \tag{2.1}$$

Weber's number depends on density, velocity, scale, and surface tension. For every bubble size, there exists a critical Weber number at which we expect to see 95 pct. under the said bubble size. It is empirically found, depends on the flow type, and is usually around 0.585 to 2.35 [6].

$$We_{critical} = \frac{\rho \bar{v}^2 D_{max}}{\gamma} \tag{2.2}$$

When we know our target Weber number and try to achieve it, a second challenge appears when we examine velocity term $\bar{v}$ in (2.2). It is

defined as the average value across the whole flow field of the squares of velocity differences over a distance equal to D_{max} ! This becomes even more problematic when the bubble size is comparable to the boundary layer thickness. Therefore the author expresses velocity (2.3) in terms of energy input by assuming isotropic homogeneous turbulence.

$$\bar{v}^2 = C_1(\epsilon D_{max})^{2/3} \tag{2.3}$$

where ϵ is the turbulence kinetic energy (TKE) dissipation rate which is a fundamental parameter indicative of the strength of turbulence measured in W/kg. With more assumptions like small Vi, experimentally found constants, and accounting for the statistical nature of bubble breakup maximum bubble size can be expressed as (2.4):

$$D_{max95} = 0.725\left(\frac{\gamma}{\rho_c}\right)^{3/5}(\epsilon)^{-2/5} \tag{2.4}$$

Two following interpretations of this result can be expressed.

1. Two key material properties - surface tension and density of continuous phase - form a ratio. Adjusting this ratio allows us to interpret the results of water models and predict how these findings will change with the density and viscosity of liquid metal.

2. Increasing turbulence dissipation rate will refine the bubbles.

3. Literature overview

3.1. Existing aluminum degassing methods

Multiple degassing methods exist, which differ technologically, but the under-laying mechanisms of hydrogen removal are always via diffusion. Suppose nothing is done to an aluminum crucible. In that case, the dissolved hydrogen moves in the direction of the concentration gradient to the free surface (assuming a lower H_2 concentration in air). Such a scenario is impractically slow in the case of an aluminum furnace with a characteristic size of 1 m. So all existing methods aim to accelerate the diffusion rate by manipulating the pressure, surface area and/ or the distance to the area of lower concentration. The four most common are listed down below:

1. Gas purging with a rotary gas injector [2] where a rotating impeller achieves gas injection and stirring. Overall, gas purging is the most researched method, and through the past 40 years [7] has gone through many iterations. It has been optimized in geometry, specifically nozzle design which can rotate and expel gas or powder to refine the gas bubbles to a certain size. The most primitive way of gas purging is gas injection via a lance that produces bubbles with the size of centimeters which has thermodynamic efficiency around 10..20 %. Finer bubbles can be achieved by using a porous plug at the end of a lance, increasing efficiency to 30..40 %. Advancement in gas purging methods came in 1966 [8] when the "Spinning Nozzle Inert Flotation" (SNIF) process was introduced. Its degassing efficiency is close to 100 % [9] as it produces millimeter-sized bubbles. The key in the SNIF process is using a stator that encloses the rotor. In the gap between the rotor and the stator, massive shear forces are created, and the gas is injected exactly there.

2. Ultrasound degassing which uses mechanical waves that create pressure oscillations in metal. When mechanical ultrasound is applied, an instantaneous variation in local pressure takes place. During the phase of low-pressure tiny gas bubbles form, which at the high-pressure phase collapse and produces shock waves. These oscillations greatly increase the mass transfer rate through rectified diffusion [10], resulting is a vastly improved diffusion rate compared to the case where nothing is done. For example, aluminum degassing for samples of 0.2 kg to 2.0 kg is in the range of 1-7 minutes depending on conditions [11]. Ultrasound degassing is very effective for small

volumes but loses applicability when the aluminum volume is scaled because ultrasound intensity drops off quickly with distance making the degassing localized only around the probe.

3. Vacuum degassing where pressure on the free surface is reduced to accelerate gas removal. When partial pressure is reduced, the maximum solubility of hydrogen drops according to Sievert's law. A practical analogy is the first opening of a carbonated drink. There CO_2 is dissolved in water and is stable in the elevated pressure of $2-3.5$ atm. The pressure is reduced to atmospheric when the bottle is opened, and CO_2 starts escaping. However, despite a high degree of saturation, if the water is not perturbed, CO_2 escapes slowly with a characteristic time of hours. That is why the vacuum degassing method is often combined with ultrasonic degassing [12] since vacuum degassing alone is too slow. For example, for an 800 g aluminum sample, the degassing process takes 20-30 minutes [11], and the duration would only increase with the aluminum volume rise. Adding another perturbation in the form of ultrasound increases process time by an order of magnitude.

4. Chemical degassing where substances are added to the melt, thus reacting with aluminum and producing gases that remove hydrogen similarly to the gas purging method. Tablet degassing works by adding compounds that react with aluminum and produce gas. For example, hexachloroethane (C_2Cl_6) is added as a solid, and various reactions [13] whose end products are in gaseous form take place. Produced gases utilize the same principle as gas purging and remove dissolved hydrogen via insoluble gases that rise to the top.

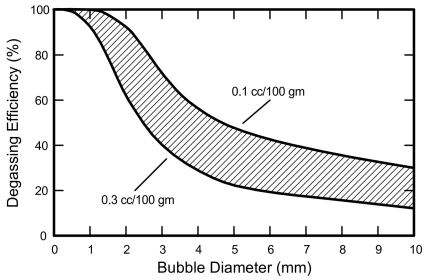

Figure 3.1: **Degassing efficiency at two hydrogen content levels** [9]

The correlation of the degassing efficiency and the degassing bubble size for a 250 kg crucible furnace is shown in Fig. 3.1. Based on this a 2 mm target is set for bubble size diameter.

3.2. Bubble formation in liquid metals

An extensive review of bubble dynamics in liquid metals is found in a review article [14] by Haas et al. It covers measurement methods, emphasizing liquid metals and discussing their shortcomings and difficulties. The most relevant to this thesis is the discussion about the bubble formation mechanism at nozzles and purging plugs.

Firstly, it is shown that the surface properties of the gas inlet dictate the bubble formation process. In the case of bubble generation through a sieve tray, wetted and non-wetted surfaces produce radically different results. Wetted sieve produces smaller bubbles that are more homogeneously dispersed through more holes [15]. Article also highlights the limits of the applied gas flow rate before bubbles from neighboring holes join together and form a blanket of gas instead of individual bubbles. Laboratory experiments in this thesis use a single orifice for gas injection, however, due to the smaller size, this wetting of the crucible walls becomes essential. If the flow is not strong enough and the gas inlet is close to a wall ($< 1\ cm$), a gas pocket might form and rise to the surface by slipping between the wall and the metal.

Secondly, bubble size is determined by both the gas flow rate and the gas inlet size. Recent article [6] collects critical Weber numbers for different turbulent flow setups. They are usually in the range of 0.585 to 2.35. The article experimentally shows a larger number of bubbles right after their birth, but in a later time, they experience coalescence and reach a stable count in the turbulent pipe flow. Bubble size spectra (number of observed bubbles vs. bubble size) follow a $-10/3$ power law.

Thirdly, gas bubble diameter moderately increases with increasing gas flow rate [16]. The average volume of a gas bubble is roughly proportional to the gas injection flow rate. Noteworthy is the fact that if the flow rate is controlled (e.g., with a mass flow controller), one can measure the frequency of the bubble detachment process and make predictions of the bubble size. Examples of frequency and flow rate correlations can be seen in this study [17].

Fourthly, gas bubble diameter depends on the injection orifice size [18]. They have investigated the dynamics of bubble formation from submerged orifices ranging from 0.04 to 0.8 mm and found different mechanisms of bubble formation compared with millimeter-range orifices. Regardless, the correlation remains the same - the smaller the orifice, the finer bubbles can be produced.

4. Experiments

Experiments are the foundation of this work, so experimental setups are introduced and described in detail in this chapter. Broadly speaking, they can be divided into experimental series with GaInSn alloy and aluminum. All measurement methods used are mentioned here for both cases. The majority of work is done with GaInSn alloy in a single setup which was adapted for a multitude of experiments. Vast majority of results and discussion are found in the next chapter nr 5.

4.1. GaInSn experimental model

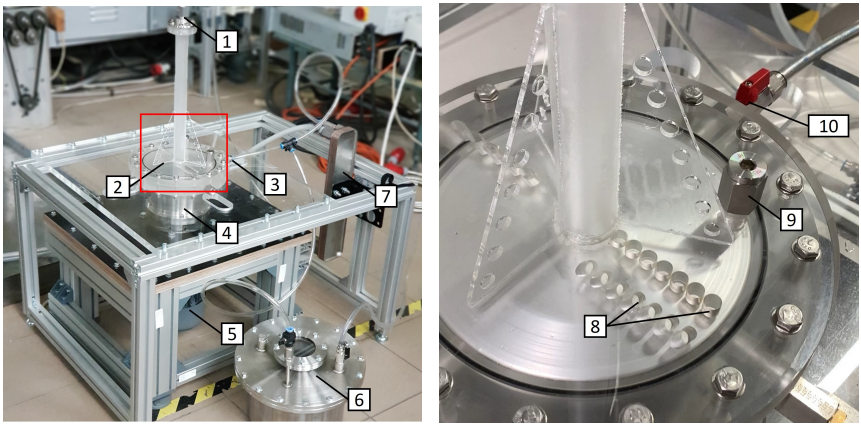

(a) **Setup** *(b)* **Closeup**

Figure 4.1: **GaInSn experimental model: 1 - inlet 2 - plexiglass vessel for GaInSn; 3 - outlet; 4 - permanent magnet rotor; 5 - electric motor; 6 - GaInSn storage; 7 - heatsink; 8 - measuring holes for UDV; 9 - argon inlet; 10 - outlet**

A scaled experimental model for the proposed degassing unit has been built to better understand the electromagnetically created flow and to validate our numerical model. The model (see Fig. 4.1) has a GaInSn reservoir designed from acrylic glass with implemented measuring holes for ultrasound Doppler velocimetry (UDV). The placement of the measuring holes is shown in Fig. 4.1b. Under the liquid container, a permanent magnet rotor is placed co-axially to the vessel and controlled by an electric

motor via variable-frequency drive. A permanent magnet rotor is magnetized radially (see Fig. 4.2b), and such a setup produces a magnetic field in the container as shown in Fig. 4.2. The model provides an option

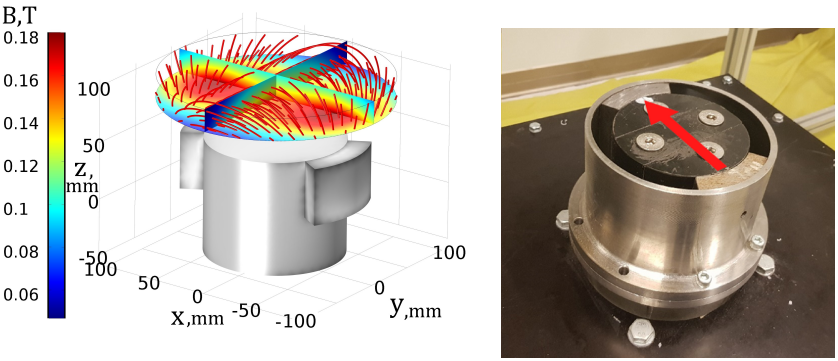

(a) **Magnetic field** *(b)* **Magnet rotor**

Figure 4.2: **Magnetic field in the container and relative position to the magnet. The red arrow indicates magnetization.**

to circulate the liquid metal through loops or restrict the stirring in the GaInSn reservoir in order to model all possible use cases. Dimensions of the reservoir are given in Table 4.1.

Table 4.1: **Dimensions of experimental and industrial system**

Type	Metal	Diam., m	Height, m	Rotor, m	gap, m
Laboratory	GaInSn	0.20	0.03	0.12	0.038
Industrial	Al	0.60	0.14	0.36	0.11

Gallium alloy GaInSn is used as the metal for the scaled model. Its properties and molten aluminum's are shown in Table 4.2. GaInSn is 2.7 times denser, has about 70 % of electrical conductivity, and has about the same dynamic viscosity as typical aluminum alloy. In the case of aluminum, the properties vary with temperature and the type of alloy used. Here we describe values just above the melting temperature. Out of all properties, alloying materials most drastically impact electrical conductivity, making it worse. That happens even in low concentrations under 1 %. There can be up to a 3 times difference in electrical conductivity between some aluminum alloys compared to pure aluminum in elemental form. This is important to us because electromagnetic forces are proportional to electrical conductivity. Alloying elements can both decrease and increase viscosity. For example dynamic viscosity of pure aluminum at melting

temperature is about $2 \cdot 10^{-}3$ Pa·s but viscosity range of aluminum alloys is from $1 \cdot 10^{-3}$ Pa·s to $4 \cdot 10^{-3}$ Pa·s.

Table 4.2: **GaInSn and aluminum properties**

Metal	$T_m, ^oC$	$\rho, kg/m^3$	$\sigma, S/m$	$\nu, m^2/s$	$\eta, Pa \cdot s$
GaInSn [19]	-19	6400	$3.46 \cdot 10^6$	$3.75 \cdot 10^{-7}$	$2.4 \cdot 10^{-3}$
Al [20] [21]	660	2391	$4.85 \cdot 10^6$	$1.55 \cdot 10^{-6}$	$2.0 \cdot 10^{-3}$

One of the features that dictate the bubble size of the injected gas in a liquid is the diameter of the injection orifice [18]. Broadly speaking, smaller bubbles can be produced by a smaller injection orifice. Industrial solution use either porous material or material with small (sub-millimeter) holes drilled into it. In this experiment, we iterated the nozzle design and reached a solution to use a medical needle with an adapter shown in Fig. 4.3b. The injection port is located close to the outer wall of the cylinder (see Fig. 4.3a) since the bubbles in this system move toward the center. Here it is also essential that the injection tip is not within the wall but protrudes into the metal to achieve maximum shear forces.

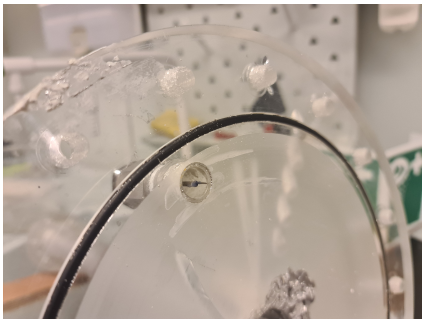

(a) **Position of the needle**

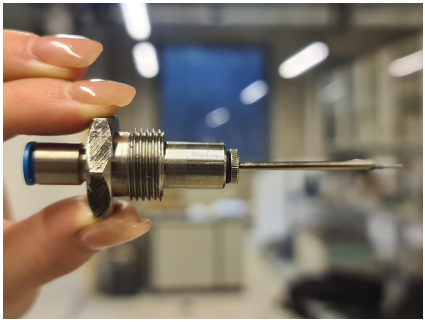

(b) **Injection adapter with the needle**

Figure 4.3: **Second iteration of the gas injection system. A 0.4 mm needle is used to inject argon bubbles into the melt.**

4.2. Experimental measuring techniques

To characterize the GaInSn experimental model, multiple parameters are measured, which include flow velocity, developed pressure, flow rate, induced power, bubble size, and bubble dynamics. In general, we want to quantify how hydrodynamics are affected by variables such as magnet rotational frequency, the geometry of the liquid metal vessel, and rotating permanent magnet machinery. To do that, multiple experimental techniques are used:

- Ultrasound Doppler velocimetry - using this method, one can measure flow velocity projection on the axis of the probe in a non-intrusive way. To reiterate, the device measures the velocity component parallel to the probe. Velocity is obtained in multiple depths, forming a profile that consists of approx. 100 points depending on settings.

- Hydrostatic pressure measurements - are taken by measuring the height of the liquid metal column with an accuracy of 2 mm. The developed pressure is equal to $\rho_{GaInSn} g \Delta h$ where the height difference is measured relative to the reference level when there is no stirring. For reference, 0.1 atm pressure produces 160 mm pressure head in GaInSn, yielding 1.2 % accuracy at this specific pressure.

- Flow rate and power measurements by analyzing dissipated heat. Metal temperature changes are measured when different magnetic field frequencies are applied. If the mass and specific heat capacity are known, and the system is thermally insulated, we can calculate the dissipated energy with Eq. $m \cdot c_p \cdot \Delta T = P \cdot t$, where c_p is the specific heat capacity of GaInSn, m is the mass of GaInSn being stirred, temperature rise over time t and P is the total power induced in the liquid metal.

- Image acquisition of bubbles in a turbulent flow is made by observing the free surface of liquid metal with a high-framerate camera. Filming metal surfaces poses some unique challenges, mainly because liquid metal is opaque and becomes a mirror when the metal surface is very clean. In this work, most filming was done on a GaInSn surface, but one experiment was performed with aluminum.

- Aluminum sample cross-section analysis is used to visualize porosity. It is possible to count the pores and their area to quantify porosity. This is the simplest method that can show the existence of excess hydrogen.

5. Results and discussion

In this section main results of the thesis are presented. Metal flow is characterized by analyzing velocity, pressure, flow rate, and power which all are obtained with GaInSn experimental model. Most measurements are also presented together with numerically modeled flow results done by the team's Ph.D. student Didzis Berenis as part of the project. Comparison to numerics is important because in later parts when we analyze TKE dissipation rate, which is the best predictor of bubble size and can not be measured experimentally in liquid metals. For that, we only rely on provided results by modeling, which, in a sense, are validated by experimental measurements we can obtain (e.g., velocity and pressure).

Gas injection experiments in GaInSn gave insight into bubble size distribution which is a rare, if not unique, finding in liquid metal. Aluminum experiments, by nature, provide fewer measurements and do more of a demonstration role. Yet they are vital because they test difficult-to-predict problems like a gas injection. Lastly, dimensionless analysis is done as a part of the technology scaling process, where the main dimensionless numbers are examined, and predictions about industrial-sized systems are made.

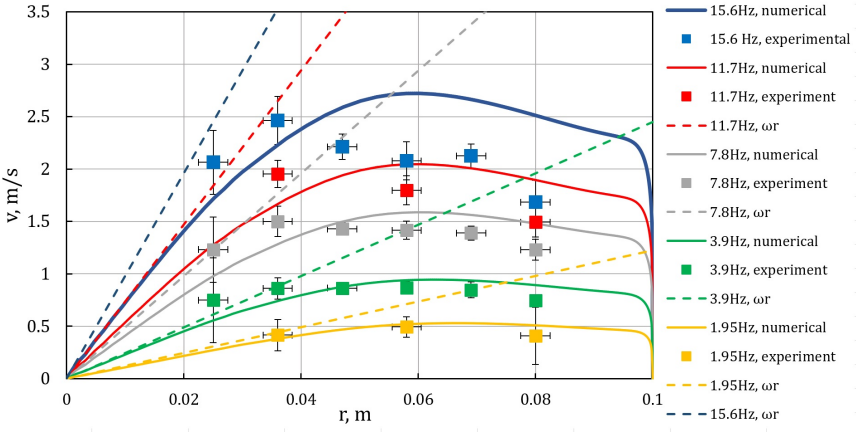

Figure 5.1: **Flow profiles at different magnet rotation frequencies. Lines represent numerical calculations, squares are experimental measurements and dashed lines are ωr - velocity of the magnetic field at a given radius. The vertical error bar is one standard deviation of flow velocity. Horizontal error bars indicate the width over which the velocity is averaged.**

Velocity measurements were possible for azimuthal flow up to 3 m/s, Which allowed us to measure flow in the applied frequency range of 2-20 Hz. Together with pressure measurements, they formed the basis of results used to validate the numerical model. Power measurements produced some inconclusive results. The discrepancy between numerical and experimental measurements was larger than for pressure and velocity. Solid aluminum cross-sections also proved to be more difficult than anticipated because of inconclusive results which were omitted in this work. Bubble size measurements worked

Tangential velocity in multiple radial positions is presented in Fig. 5.1 where experimental, numerical and magnetic field velocities are compared. Firstly, a maximum velocity in numerical calculations is observed at radial position $R = 58$ mm and in experiment in position $R = 38$ mm. At first, it seems counter-intuitive since the velocity of the traveling magnetic field is proportional to radius $v = \omega R$, so a larger velocity is expected near the outer wall. Just as unexpected is the fact that in the cases of low rotational frequency, it is observed that the fluid moves as fast as the magnetic field in the region closer to the center. Both of these findings can be explained by the inward transfer of angular momentum by the radial flow.

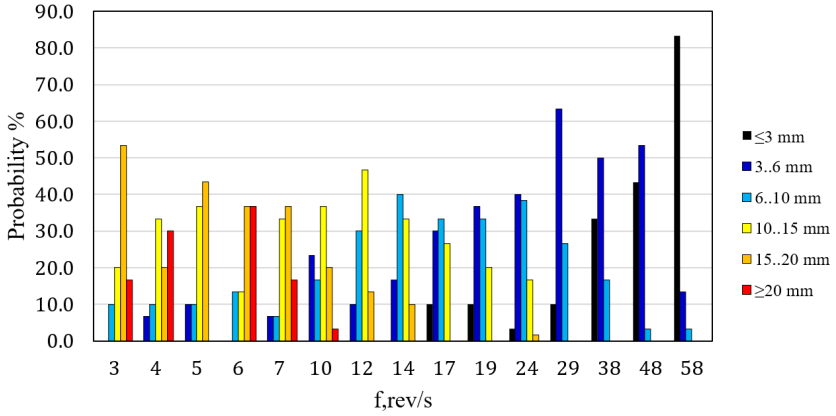

Figure 5.2: **Bubble size distribution across different stirring frequencies**

Fig. 5.2 shows bubble size distributions across the whole tested frequency range highlighting the shift to smaller bubbles denoted in darker colors. Overall the size of bubbles can span an order of magnitude regardless of the stirring frequency. This fact complicates the theoretical analysis since most of the volume of the gas could be found in relatively few large

bubbles, but most of the surface could be formed by many tiny bubbles.

Fig. 5.3 shows experimentally mean bubble size decreased from 16 to 2.3 mm reaching the minimum desired threshold (ideally 1 - 2 mm bubble size should be achieved) [9]. Numerical results predict a similar reduction in size from 22 to 1.2 mm with increasing frequency.

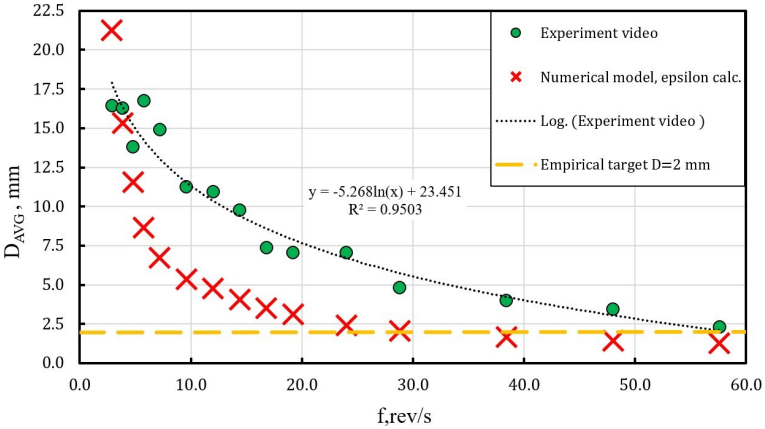

Figure 5.3: **Mean bubble size a function magnet rotational frequency. Experimentally measured value comparison to analytical/numerical calculations. The dashed orange line indicates the empirical target.**

Main system parameters and dimensionless numbers are collected in Table 5.1. The GaInSn model, laboratory aluminum model, and aluminum industry prototype are compared here. The linear size-wise aluminum prototype is three times larger, and its volume is around 50 times bigger than laboratory experiments. Velocity predicted by numerical modeling is 5 m/s for the GaInSn model and 6 m/s for the industry prototype. Due to the larger size, the Reynolds number still will be significantly larger in the industry prototype. Used frequencies on the larger scale are naturally smaller. Due to lower frequencies and larger size, skin depth is bigger in absolute terms. Relative to the smallest dimension, this ratio is more or less constant since it is one of the main limiting factors for electromagnetic stirring. Hartmann's number is bigger than unity in all cases, so electromagnetic forces dominate viscous forces. Stuart's number is smaller than one in all cases, with the largest value for the industrial prototype. This indicates that electromagnetic forces, at best, are comparable to inertial forces. Magnetic Reynolds number is around unity for laboratory models and 10^1 for the prototype. This means that the velocity of the conducting fluid will significantly impact the magnetic field distribution. Maximum values of dimensionless frequency are 15 for the laboratory model and 34

Table 5.1: **Dimensionless numbers of laboratory model and numerical prototype**

-	Unit	GaInSn model	Al lab model	Al industry prototype
R	m	0.10	0.05	0.30
V	L	1	1	50
u	m/s	5	2.5	6
f	Hz	57.6	57.6	10
Re	-	$4.4 \cdot 10^5$	$1.5. \cdot 10^5$	$1.0 \cdot 10^6$
Re_m	-	$2.1 \cdot 10^0$	$7.6 \cdot 10^{-1}$	$1.1 \cdot 10^1$
Ha	-	$6.1 \cdot 10^2$	$3.7 \cdot 10^2$	$2.2 \cdot 10^3$
N	-	$3.2 \cdot 10^{-2}$	$1.3 \cdot 10^{-1}$	$7.3 \cdot 10^{-1}$
Pe	-	$1.3 \cdot 10^8$	$3.1 \cdot 10^7$	$4.5 \cdot 10^8$
Ω_D	-	$1.5 \cdot 10^1$	$5.6 \cdot 10^0$	$3.4 \cdot 10^1$
δ	m	0.037	0.030	0.072
ε	W/kg	5	N/A	1
D_{max}	mm	2.2	10	5
τ	s	13	N/A	26

for the industrial prototype. That means diffusion of the magnetic field can not keep up with the rapid changes of the magnetic field. This is on par with literature where optimal dimensionless frequency for maximum energy transfer is around $\Omega_D = 10..50$. The TKE dissipation rate in the industry prototype was lower than in the laboratory experiment (values in bulk). Thus the predicted bubble size is around 5 mm. Characteristic mixing time rises with the size, and it is two times longer for the industry prototype. This indicates that permanent magnet machines work well as electromagnetic stirrers in this setting. This is also supported by the Péclet number, which tells us that forced convection will dominate the mass transfer.

6. Conclusions

Most of the tasks were carried out successfully, and the thesis objectives were achieved. In the process following conclusions were made:

1. Bubbles can be refined by an electromagnetically created turbulent flow. Experiments imaging the GaInSn surface prove bubble size reduction with more intense stirring.

2. The bubble size in metal flow is correlated to flow condition, mainly ϵ -turbulent kinetic energy dissipation rate. Numerical models providing ϵ values are validated using experimentally measurable quantities such as velocity and pressure.

3. Author proposes a method for scaling the bubble refinement problem to aluminum. Numerical modeling tools can calculate the dissipation, which, together with empirical formulas, are used to predict the bubble size in aluminum.

4. Laboratory scale experiments with aluminum indicate significant bubble behavior changes when stirring is applied. Imaging the free surface showed bubble size reduction.

5. The developed pressure head is high enough for the system to work as an electromagnetic pump. This is an added benefit that none of the existing degassing methods has.

6. Iron yokes can be used as a cost-effective tool as magnetic flux concentrators even on rotating permanent magnet machinery. This setup provides at least a 30 % pressure increase which means more intensive flow or the ability to use 27 % less magnetic material for the same hydrodynamic performance.

7. Power measurements show how much energy can be transferred to the system by EM forces. They proved that the limit in frequency was not reached in the tested frequency range. This is useful for building and scaling EM machines for metal stirring.

8. Despite producing a small enough bubble, vertical setup proved to have very poor bubble residence time.

6.1. Publications and participation in conferences

Publications

1. R. Baranovskis, D. Berenis, I. Grants, A. Bojarevics, T. Beinerts, M. Milgravis
   Contactless Aluminum Degassing System—GaInSn Model Experiments and Numerical Study
   Journal of Sustainable Metallurgy (2021)

2. D. Berenis, R. Baranovskis, I. Grants, T. Beinerts, A. Bojarevics,
   Permanent magnet bottom-stirred swirling flow in coaxial shallow cylindrical containers
   Physics of Fluids 33 (5), (2021)

3. I. Grants, R. Baranovskis
   Experimental observation of metal-electrolyte interface stability in a model of liquid metal battery
   Magnetohydrodynamics 57 (2), (2021)

4. R. Baranovskis, M. Sarma, M. Scepanskis, T. Beinerts, A. Gaile, S. Eckert, D. Räbiger, E.H. Lehmann, K. Thomsen, P. Trtik
   Investigation of Particle Dynamics and Solidification in Two-Phase System by Neutron Radiography
   Magnetohydrodynamics 56 (1), (2020)

5. I. Kaldre, C. Wang, R. Baranovskis
   Experimental investigation of weld pool flow under external DC magnetic fieldy
   Magnetohydrodynamics 55 (4), (2020)

6. I. Kaldre, A. Bojarevics, T. Beinerts, R. Baranovskis, R. Nikoluskins, M. Milgravis, M. Kalvans
   Contactless electromagnetic method for aluminium degassing
   IOP Conference Series: Materials Science and Engineering, 424 (1), (2018)

7. T. Beinerts, A. Bojarevics, R. Baranovskis, M. Milgravis, I. Kaldre.
   Permanent magnet dipole stirrer for aluminium furnaces
   IOP Conference Series: Materials Science and Engineering, 424 (1), (2018)

8. A. Bojarevics, R. Baranovskis, I. Kaldre, M. Milgravis, T. Beinerts
Two cylinder permanent magnet stirrer for liquid metals
IOP Conference Series: Materials Science and Engineering, 228 (1), (2017)

International conferences

1. 12th International PAMIR International Conference - Fundamental and Applied MHD July 04 – 08, 2022, Krakow, Poland
R. Baranovskis, D. Berenis, I. Grants, A. Bojarevics and T. Beinerts
Bubble dispersion in liquid metal flow.

2. 2022 CaNAl Alumina Summer School, July 13 – 16, 2022, Trondheim, Norway
R. Baranovskis, D. Berenis, I. Grants, A. Bojarevics and T. Beinerts
Novel electromagnetic degassing system

3. Electromagnetic processing of materials 2021, June 13 - 17, 2021
R. Baranovskis, D. Berenis, I. Grants, A. Bojarevics and T. Beinerts
Experimental modelling of permanent magnet stirrer for aluminum degassing

4. XIX International UIE Congress on Evolution and New Trends in Electrothermal Processes (UIE 2021), September 01 – 03, 2021, Pilsen, Czech Republic
R. Baranovskis, D. Berenis, I. Grants, A. Bojarevics and T. Beinerts
New contactless aluminum degassing system - GaInSn model experiments with a numerical study

5. 14th Virtual Congress WCCM and ECCOMAS 2020, January 11 - 15, 2021.
I.Grants, R. Baranovskis, A. Bojarevics and T. Kalnins
Liquid metal battery instability experiment using two-layer gallium-electrolyte model

Patents

1. LV15144 ELEKTROVADOŠU METĀLISKU UN PUSVADĪTĀJU KAUSĒJUMU MAISĪŠANAS IERĪCE

Andris BOJAREVIČS (LV), Jurijs GEĻFGATS (LV), Toms BEINERTS (LV), Matīss KALVĀNS (LV), Reinis BARANOVSKIS (LV)

2. LVP2021000051 IEKĀRTA BEZKONTAKTA PLŪSMAS IEROSINĀŠANAI ELEKTROVADOŠOS ŠĶIDRUMOS
Andris BOJAREVIČS (LV), Jurijs GEĻFGATS (LV), Toms BEINERTS (LV),
Reinis BARANOVSKIS (LV)

6.2. Further research

Bubble dispersion in liquid metals has a larger impact than just liquid metal degassing. Other important areas include:

1. Steel furnaces use bubble columns for stirring and decarbonization. There locally rising bubbles can create a flow throughout the whole of the furnace. Bubble dynamics of this process have been researched numerically [22] and experimentally [23]. Steel furnaces also do desulfurization [24] where chemical agents are added on top or injected through a lance via carrier gas in the melt. The latter process shares the aims of bubble dispersion similar to aluminum degassing.

2. Production of hydrogen from natural gas pyrolysis has recently gained interest in research and energy technology. Pyrolysis of natural gas has not yet been commercialized under the aspect of hydrogen production. Still, when the carbon by-product of this process can be used for material production, the produced hydrogen has a low carbon footprint. This article [25] reviews the literature on the state of the art of methane natural gas pyrolysis process developments and attempts to assess the technology readiness level (TRL). Introducing electromagnetic stirring to bubble reactors could boost their efficiency and alter the maximum feasible size of reactors. Metal does not take place in the reaction, it works as a catalyst and ensures the right temperature and oxygen-free environment for reactions to occur. Without a catalyst (like Nickel), the decomposition still takes place, albeit at higher temperatures. Different metals and molten salts have been proposed as catalyst [26]. Aluminum could be hypothetically used, thus sharing a similar problem as this work of "how to break and disperse bubbles in liquid metal".

3. Removal of inclusions using microbubbles is a topic of interest in the aluminum and steel industry [27]. They remove the inclusion

by collecting them to the surface/liquid interface of the bubble and then transporting the attached inclusion to the top, where they can be skimmed. The problem is how to create a dispersed cloud of microbubbles such they do not merge with each other. Quoting the authors: *"... the formation of microbubbles is indeed possible in liquid metal systems, provided one has the following elements in place: a rapidly shearing flow system, strong convective flows, a dispersed flow of bubbles, plus abundance of the kinetic energy of turbulence."*. The studied electromagnetic technology in work can be used to create a turbulent flow in liquid metal systems.

A couple of ideas could be used to improve upon the concept of studied technology.

1. First is improvement in geometry where multiple optimization options seem possible. Increasing container height in the existing setup would improve residence time for the bubbles in the melt. Numerical modeling results showed that in the inlet and outlet, there is a significantly higher TKE dissipation rate. Similarly, a constriction of the channel cross-section area could be applied at the gas injection position. Lastly, the cylindrical container with a liquid metal setup can be shifted 90 degrees to a place that resembles a coin standing on the edge. That would have no effect on EM forces and fluid dynamics in single-phase flow but would drastically change the bubble path in the metal when gas is injected.

2. Second is the usage of not one but two rotating magnets, which are counter-rotating. This setup is expected to form a similar flow between two coaxial rotating disks [28] (such a setup has also been studied on a large scale with liquid metal in von Kármán Sodium experiment [29]). This causes regions of opposite azimuthal flow near the bottom and top walls. Even though mean flow velocities are lower than compared to one magnet (or one rotating wall), this setup produces high shear forces in the plane, which slices the setup horizontally in the middle.

3. Thirdly, the obstruction could be added to the flow. Adding an obstacle in rapid moving flow would cause a turbulent wake behind it. That area might be a good candidate for gas injection. Yet, in the case of aluminum, the object would have to be from ceramic material so that it would be prone to erosion. However, a strong localized magnetic field is an intriguing way to create a virtual obstruction. An example of this is seen in an article by Román [30] where they experimentally study vortex wakes produced by localized Lorentz

force in a shallow layer of electrolyte. Even though a stationary magnetic field brakes the fluid, they have shown that such magnetic obstacles can, for example, aid the heat transfer by making the flow more turbulent. Such a concept could theoretically be applied near the gas injection zone to make the flow more turbulent and hopefully aid bubble breaking process.

6.3. Author's contribution

Due to the nature of experiments in this research area, most of them are performed in a team. The author of this thesis took part in and managed all of the laboratory experiments in this study. In total, there were more than 30 GaInSn experiments and 5 aluminum experiments in the laboratory.

The project team manufactured the industrial prototype and organized the test in the aluminum plant. The author contributed to the design of the permanent magnet rotor by magnet field modeling, ferromagnetic yoke calculations, and stray magnetic field estimates. The author also took part in the design of the permanent magnet rotor assembly process, which consists of 216 individual magnets, which had to be done in-house due to the complexity of the problem. The author was doing flow imaging and aluminum sample acquisition in industrial aluminum tests.

The author performed magnetic field calculations for iron yoke optimization using the software COMSOL Multiphysics. Flow modeling was performed by Didzis Berenis within the ERDF project. The prototype of the industrial degassing unit was developed by the project team.

Dimensionless number calculations and their analysis in the scaling process are solely done by the author of the thesis.

In the aforementioned publications, authorship order indicates the relative contribution of each author.

References

[1] D. E. J. Talbot, Effects of hydrogen in aluminium, magnesium, copper, and their alloys, International Metallurgical Reviews 20 (1) (1975) 166–184. doi:10.1179/imtlr.1975.20.1.166.

[2] E. Mancilla, W. Cruz-Méndez, I. E. Garduño, C. González-Rivera, M. A. Ramírez-Argáez, G. Ascanio, Comparison of the hydrodynamic performance of rotor-injector devices in a water physical model of an aluminum degassing ladle, Chemical Engineering Research and Design 118 (2017) 158 – 169. doi:10.1016/j.cherd.2016.11.031.

[3] D. P. N. Anyalebechi, Techniques for determination of the hydrogen content in aluminium and its alloys—a review, Cast Metals 3 (4) (1990) 182–201. doi:10.1080/09534962.1990.11819039.

[4] T. Wairegi, J. Grace, The behaviour of large drops in immiscible liquids, International Journal of Multiphase Flow 3 (1) (1976) 67–77. doi:10.1016/0301-9322(76)90036-7.

[5] J. O. Hinze, Fundamentals of the hydrodynamic mechanism of splitting in dispersion processes, AIChE Journal 1 (3) (1955) 289–295. doi:10.1002/aic.690010303.

[6] W. Zhao, H. Wang, R. Bai, W. Wei, H. Wang, Bubble characteristics and turbulent dissipation rate in horizontal bubbly pipe flow, AIP Advances 11 (2) (2021) 025125. doi:10.1063/5.0035816.

[7] L. Zhang, X. Lv, A. T. Torgerson, M. Long, Removal of impurity elements from molten aluminum: A review, Mineral Processing and Extractive Metallurgy Review 32 (3) (2011) 150–228. doi:10.1080/08827508.2010.483396.

[8] A. G. Szekely, Degassing molten metals, Google Patents, US Patent 3,227,547 (1966).

[9] G. K. Sigworth, E. M. Williams, D. C. Chesonis, Gas Fluxing of Molten Aluminum: An Overview, Springer International Publishing, Cham, 2016, Ch. Furnaces, Melting, Fluxing, and Alloying, pp. 65–70. doi:10.1007/978-3-319-48228-6_9.

[10] T. Leong, M. Ashokkumar, S. Kentish, The Growth of Bubbles in an Acoustic Field by Rectified Diffusion, Springer Singapore, Singapore, 2016, Ch. Fundamental Aspects, pp. 69–98. doi:10.1007/978-981-287-278-4_74.

[11] H. Xu, Q. Han, T. T. Meek, Effects of ultrasonic vibration on degassing of aluminum alloys, Materials Science and Engineering: A 473 (1) (2008) 96 – 104. doi:10.1016/j.msea.2007.04.040.

[12] H. Xu, X. Jian, T. Meek, Q. Han, Ultrasonic Degassing of Molten Aluminum under Reduced Pressure, John Wiley and Sons, Ltd, 2013, Ch. Melt Quality: Degassing, Filtering, and Analysis, pp. 246–250. doi:10.1002/9781118647783.ch30.

[13] K. Strauss, Chapter 7 - the treatment of aluminium and aluminium alloys, in: K. Strauss (Ed.), Applied Science in the Casting of Metals, Pergamon, 1970, pp. 268 – 270. doi:10.1016/B978-0-08-015711-5.50018-X.

[14] T. Haas, C. Schubert, M. Eickhoff, H. Pfeifer, A review of bubble dynamics in liquid metals, Metals 11 (4) (2021). doi:10.3390/met11040664.

[15] T. Loimer, G. Machu, U. Schaflinger, Inviscid bubble formation on porous plates and sieve plates, Chemical Engineering Science 59 (4) (2004) 809–818. doi:10.1016/j.ces.2003.10.020.

[16] G. Kocamustafaogullari, W. Huang, J. Razi, Measurement and modeling of average void fraction, bubble size and interfacial area, Nuclear Engineering and Design 148 (2) (1994) 437–453. doi:10.1016/0029-5493(94)90124-4.

[17] S. Arias, R. González-Cinca, X. Ruiz, L. Ramírez-Piscina, J. Casademunt, Characterization of the performance of an injector for the controlled generation of microbubbles, 59th International Astronautical Congress 2008 proceedings (09 2008).

[18] E. Mohseni, J. Jose Kalayathine, S. F. Reinecke, U. Hampel, Dynamics of bubble formation at micro-orifices under constant gas flow conditions, International Journal of Multiphase Flow 132 (2020) 103407. doi:10.1016/j.ijmultiphaseflow.2020.103407.

[19] S. Cheng, Z. Wu, Microfluidic electronics, Lab on a chip 12 (2012) 2782–91. doi:10.1039/c2lc21176a.

[20] A. Dinsdale, P. Quested, The viscosity of aluminium and its alloys—a review of data and models: Special section: Proceedings of the 2003 international symposium on liquid metals (guest editors: P. d. lee, a. mitchell, a. jardy, j.-p. bellot), Journal of Materials Science 39 (12 2004). doi:10.1023/B:JMSC.0000048735.50256.96.

[21] R. Brandt, G. Neuer, Electrical resistivity and thermal conductivity of pure aluminum and aluminum alloys up to and above the melting temperature, International Journal of Thermophysics 28 (2007) 1429–1446. doi:10.1007/s10765-006-0144-0.

[22] G. Chen, S. He, Numerical simulation of argon–molten steel two-phase flow in an industrial single snorkel refining furnace with bubble expansion, coalescence, and breakup, Journal of Materials Research and Technology 9 (3) (2020) 3318–3329. doi:10.1016/j.jmrt.2020.01.026.

[23] X. Cui, Y. Xue, D. Zhao, S. Wang, F. Guo, Physical modeling of bubble behaviors in molten steel under high pressure, High Temperature Materials and Processes 40 (1) (2021) 471–484. doi:doi:10.1515/htmp-2021-0045.

[24] V.-V. Visuri, T. Vuolio, T. Haas, T. Fabritius, A review of modeling hot metal desulfurization, Steel Research International 91 (2020) 1900454. doi:10.1002/srin.201900454.

[25] S. Schneider, S. Bajohr, F. Graf, T. Kolb, State of the art of hydrogen production via pyrolysis of natural gas, ChemBioEng Reviews 7 (5) (2020) 150–158. doi:10.1002/cben.202000014.

[26] B. J. Leal Pérez, J. A. Medrano Jiménez, R. Bhardwaj, E. Goetheer, M. van Sint Annaland, F. Gallucci, Methane pyrolysis in a molten gallium bubble column reactor for sustainable hydrogen production: Proof of concept and techno-economic assessment, International Journal of Hydrogen Energy 46 (7) (2021) 4917–4935. doi:10.1016/j.ijhydene.2020.11.079.

[27] T. Engh, G. Sigworth, A. Kvithyld, Principles of Metal Refining and Recycling, Oxford University Press, 2022.

[28] K. Stewartson, On the flow between two rotating coaxial disks, Mathematical Proceedings of the Cambridge Philosophical Society 49 (2) (1953) 333–341. doi:10.1017/S0305004100028437.

[29] R. Monchaux, M. Berhanu, S. Aumaître, A. Chiffaudel, F. Daviaud, B. Dubrulle, F. Ravelet, S. Fauve, N. Mordant, F. Pétrélis, M. Bourgoin, P. Odier, J.-F. Pinton, N. Plihon, R. Volk, The von kármán sodium experiment: Turbulent dynamical dynamos, Physics of Fluids 21 (3) (2009) 035108. doi:10.1063/1.3085724.

[30] J. Román, A. Figueroa, S. Cuevas, Wake patterns behind a magnetic obstacle in an electrolyte layer, Magnetohydrodynamics 53 (2017) 55–66. doi:10.22364/mhd.53.1.7.

Acknowledgments

This work was financially supported by the ERDF project "Electromagnetic technology for aluminum degassing proces" with No. 1.1.1.1/18/A/149 and by the University of Latvia Foundation stipend for Ph.D. students in natural sciences. In the final year, the work was also backed by the project "Strengthening of the capacity of doctoral studies at the University of Latvia within the framework of the new doctoral model", identification No. 8.2.2.0/20/I/006.

I am thankful to my colleagues who directly or indirectly, were involved in my endeavors. Firstly, my thesis supervisor Dr. Ilmars Grants who provided excellent help regarding the theoretical aspects of the work. The discussion about physics assisted tremendously with understanding the nuances of physical processes taking place and helped me structure the thesis. Didzis Berenis developed a multi-physics numerical model of the experimental system used in this work. All of the numerical calculations involving fluid dynamics were performed by him and allowed him to gain insights into things that could not be measured in the system. Experimentally I was helped with video capture by Matīss Kalvānas, which was crucial in imaging the surface of GaInSn and aluminum. Mikus Milgrāvis assisted experimentally, contributing to many of the 30+ experiments carried out. Dr. Toms Beinerts organized collaboration between laboratory and aluminum industry partners. NTNU's professor Robert Fritzsch consulted me on aluminum degassing from the industry's point of view Lastly, I am glad to be helped by my life partner Antra Gaile. She not only supported me emotionally but also dealt with the hardest of LaTeX problems.

NATIONAL DEVELOPMENT PLAN 2020

EUROPEAN UNION
European Social Fund

INVESTING IN YOUR FUTURE